Chemical Geology 619 (2023) 121323

Contents lists available at ScienceDirect

Chemical Geology

journal homepage: www.elsevier.com/locate/chemgeo

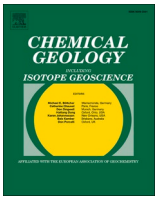

Rare earth element signature modifications induced by differential acid alteration of rocks in the Iberian Pyrite Belt

Javier Cuadros [a,*], Christian Mavris [a], Jose Miguel Nieto [b]

[a] Natural History Museum, Cromwell Road, London SW7 5BD, UK
[b] Department of Earth Sciences, University of Huelva, 21071 Huelva, Spain

ARTICLE INFO

Editor: Karen Johannesson

Keywords:
Acid alteration
Iberian Pyrite Belt
Rare Earth elements
Tracers

ABSTRACT

The efficient use of REE as tracers of weathering processes requires further data acquisition to establish robust connections between mechanisms, mineral assemblages and REE concentration patterns. Here, results are provided corresponding to rocks from four locations in the Iberian Pyrite Belt that were altered with different intensity by sulfuric fluids. The acidic alteration was mild (pH 5–7) in Calañas and El Villar, while strong (pH below 3 to 5) in Quebrantahuesos and Tharsis. The main REE reservoir before alteration were phyllosilicates (and plagioclase/feldspar in El Villar only). Mild alteration generated mainly kaolinite while illite and some plagioclase/feldspar were preserved. Mildly altered rocks approximately preserved the relative REE concentrations of their precursors, interpreted as indicating a low fluid/rock ratio environment where binding sites in minerals outnumbered those in fluids. Strong acid alteration produced alunite, jarosite, beudantite and goethite, with partial illite preservation. Where illite and/or goethite were major minerals, this alteration generated REE patterns enriched in light REE over heavy REE or did not modify the relative REE concentrations of the original rock. However, samples where REE concentrations were controlled by alunite or jarosite had LREE > > HREE. In alunite the maximum concentration corresponded to Nd and Sm. In jarosite concentrations decreased from La to Lu, except that a positive Eu anomaly was preserved from the precursor. These REE concentration patterns are interpreted as due to crystallographic factors, controlled by the best fit of REE with charge 3+ in the 12-fold coordination site of K in jarosite and alunite. This site is larger in jarosite and fits La best, whereas the smaller site in alunite best fits Nd and Sm. Goethite REE signature is variable, perhaps due to two formation routes, (1) silicates ➔ goethite and (2) silicates ➔ jarosite ➔ goethite. Our interpretations of REE concentration in alunite, jarosite and goethite are novel and provide new routes to further develop REE as tracers of acid alteration processes.

1. Introduction

REE are used as tracers of geological, geochemical and mineral processes. REE relative concentrations are modified contrastingly by processes of different characteristics due to their different ionic charge/radius ratios or possible valence state of Ce and Eu ($Ce^{3+,4+}$ and $Eu^{2+,3+}$) (Chakhmouradian and Wall, 2012). Although the general rules giving rise to the differential behavior of REE are reasonably understood and allow accurate tracing of igneous processes, there is still much to learn about how they apply or are modified in sedimentary and diagenetic environments and conditions (McLennan, 1989; Laveuf and Cornu, 2009). As a consequence, the utility of REE as tracers of the entire range of possible processes is still limited.

In rock weathering processes, one first interaction affecting the relative concentration of REE is the competition between the solid and liquid phases for these elements. Such a competition depends much on the composition of the altering fluids. Acidic fluids are more efficient than neutral ones in dissolving minerals and thus can release REE more quickly and potentially less selectively into solution (Inguaggiato et al., 2017). Different anionic species in solution (OH^-, SO_4^{2-}, Cl^-, etc.) bind to REE with different strength depending on the particular charge/radius ratio of the particular REE. As a result, dissolved anionic species compete with existing or newly precipitated minerals for REE with different efficacy. REE relative concentration in minerals during alteration processes may be further complicated with mineral segregation, as fine-grained minerals are translocated more easily than coarse ones

* Corresponding author at: Natural History Museum, Cromwell Road, London SW7 5BD, UK.
E-mail addresses: j.cuadros@nhm.ac.uk (J. Cuadros), christian.mavris@gmail.com (C. Mavris), jmnieto@uhu.es (J.M. Nieto).

https://doi.org/10.1016/j.chemgeo.2023.121323
Received 23 August 2022; Received in revised form 21 November 2022; Accepted 11 January 2023
Available online 13 January 2023

(McLennan, 1989).

During weathering processes, fine-grained minerals retain the greater portion of REE (McLennan, 1989). This is due partly to the smaller crystals (and greater number of incompletely bonded atoms) and partly to mineralogy. The large ionic charge/radius ratios of REE cause them to bind firmly to incompletely bonded, negatively charged atoms. This is the case of phyllosilicates, which have a prevalent negative charge in their structure that allows REE adsorption on both interlayer space and external surface (Kynicky et al., 2012). Given the large surface area of phyllosilicates, they frequently control REE concentrations in weathering environments (Liu et al., 2021 and references therein; Andrade et al., 2022). Indeed, phyllosilicates are economic deposits of REE in lateritic environments, where concentrations reach 0.05–0.2 wt % of total REE oxides (Borst et al., 2020). Goethite and Fe oxides (and Mn oxides and oxyhydroxides) can also retain a substantial amount of REE, greater if the crystal order is lower and the particle size smaller (Liu et al., 2021 and references therein), indicating that REE lodge preferentially on external sites rather than within the oxide lattice (Laveuf and Cornu, 2009). In acidic alteration, newly formed minerals typical of these environments, such as alunite and jarosite, are frequently also fine grained and can compete successfully for the retention of REE, even if important REE fractionation may occur (Terekado and Fujitani, 1998; Deyell et al., 2005; Welch et al., 2009). Phyllosilicates do not have a strong tendency to segregate REE because they bind to clay surfaces through ionic bonds and all have the same ionic charge (with the exception of Ce^{4+} in oxidizing conditions and Eu^{2+} in reducing conditions; Roaldset, 1973; McLennan, 1989; Prudêncio et al., 1989). The decreasing ionic radius with increasing atomic number, however, means that weathering causes some segregation because light REE (LREE) are less strongly bound to phyllosilicate surfaces than heavy REE (HREE) (Kynicky et al., 2012). Similar possible segregation effects are not established with certainty for products of acid alteration such as Fe oxides and hydroxyoxides, jarosite or alunite. Phosphates can greatly concentrate REE and control their distribution and concentration in rocks (Chakhmouradian and Wall, 2012). Because they are resilient minerals, their contribution can be especially relevant in acid-altered rocks, where they can be preserved (Deyell et al., 2005). All the individual effects mentioned above from mineralogy, mineral translocation, fluid composition and fluid pH, combine to generate the REE patterns of alteration products. In soils, organic matter also competes with mineral phases and fluids for REE, introducing one more avenue of REE pattern modification (Laveuf and Cornu, 2009) that is not developed here as not relevant to this contribution.

This study investigates the REE signatures of rocks produced by acidic alteration in some locations of the Riotinto mining district (Huelva, SW Spain). Rocks from several sites were subjected to acidic alteration of different intensity. Comparison between the REE patterns of the acidic alteration products and of their precursors provides insights on how the acid alteration processes and the mineralogy of the products combine to shape the REE patterns of these products. Such insights contribute to a more reliable use of REE as tracers of silicate alteration processes in neutral to strongly acidic conditions.

2. Geological setting

The samples are from four localities in the Iberian Pyrite Belt (Calañas, El Villar, Quebrantahuesos and Tharsis; Fig. S1), which have common elements in their geological histories but with important differences. They have been thoroughly described in Mavris et al. (2018). The parent rocks belong to an Upper Palaeozoic (Late Famennian-Visean) volcano-sedimentary complex including both siliciclastic sediments and mafic and felsic volcanics, which underwent hydrothermal alteration associated to the emplacement of a large amount of massive sulfide orebodies contemporaneously to deposition (Toscano et al., 2014). Later, Miocene erosion and subaerial exposition caused the oxidation of pyrite-rich orebodies, which resulted in the generation of mild to extreme acidic fluxes that leached the surrounding rocks for over 20 My (Essalhi et al., 2011). The resulting mineral assemblages are strongly controlled by the intensity of the local acidic alteration.

The Calañas (C) outcrop is located in a sequence of acidic tuffs. The intense hydrothermal alteration associated with the sulfide mineralization event generated a mineralogy consisting mainly of quartz and illite. The acidic alteration of this sequence is moderate and kaolinite appears as an alteration product of illite.

The El Villar section (EV), located west of the Riotinto mine, is a sequence of basic volcanics (basalts) with minor felsic rocks (rhyolites and dacites), all hydrothermally altered during sulfide mineralization. The samples studied here cover a 20 m horizontal sequence with a generally increasing acid alteration ranging from inexistent or nearly so (plagioclase is abundant) to moderate, where kaolinite is abundant.

The Quebrantahuesos (Q) area is located in the Cerro Colorado open pit, within the Riotinto mines. The samples were collected from materials on top of the Quebrantahuesos-Salomon orebody (Adamides, 2013), now disappeared due to further mining. They were originally a sequence of felsic porphyritic volcanic rocks and tuffs that were first hydrothermally altered to chloritic porphyry, rich in chlorite and quartz, during polymetallic sulfide emplacement (Adamides, 2013; Martin-Izard et al., 2015). These rocks were situated below or near the pyrite body that generated the altering acidic fluids. The acidic alteration was very intense and produced assemblages with abundant quartz, alunite, minor illite and some jarosite/beudantite, hematite and goethite.

The Tharsis (TH) outcrop is a highly deformed and altered sequence of shales with minor felsic volcanics and small lenticular masses of sulfides. Hydrothermal alteration associated with the emplacement of the sulfide masses generated quartz, kaolinite and illite in the country rock shales. The acidic alteration progressed substantially and in the shales there is abundant quartz, with kaolinite, illite, sulfates and goethite, while the sulfide lenses were altered mainly to goethite and jarosite/beudantite (Capitán et al., 2003).

3. Materials and methods

3.1. Sample collection

The samples were collected between September 29 and October 3 of 2014. The goal of the study was to investigate Earth analogs for Martian rocks from acidic alteration environments (Mavris et al., 2018), which determined the selection of sites and samples. The locations of the points from where the samples originated are indicated in Fig. 1, with the intention of providing their relative positions within each site. The sites from Calañas are not provided because only two samples were collected, several meters apart. All specimens were sampled from vertical cuts, a few centimeters below the exposed surface, to avoid contamination with soil or wind-deposited material. The only exception is sample QX in Quebrantahuesos, which was collected from a rock displaced out of context, and thus does not appear in Fig. 1.

3.2. Experimental methods

All experiments were carried out at the Natural History Museum, London. The samples were crushed in a mechanical jaw crusher and then ground, first with a planetary agate mill and then by hand to a fine powder with a mortar and pestle. They were then sieved and the fraction <100 μm was collected for analysis. The <2 μm fraction of the rocks was obtained by dispersion in deionized water and centrifugation, then concentrated by further centrifugation, dried at ~60 °C in an oven, and gently ground with a mortar and pestle.

3.2.1. XRD analysis

The bulk samples (< 100 μm) were analyzed using XRD for their whole-rock mineralogy in a PANalytical X'Pert Pro diffractometer. They were side-loaded to minimize preferred orientation. Measurements were

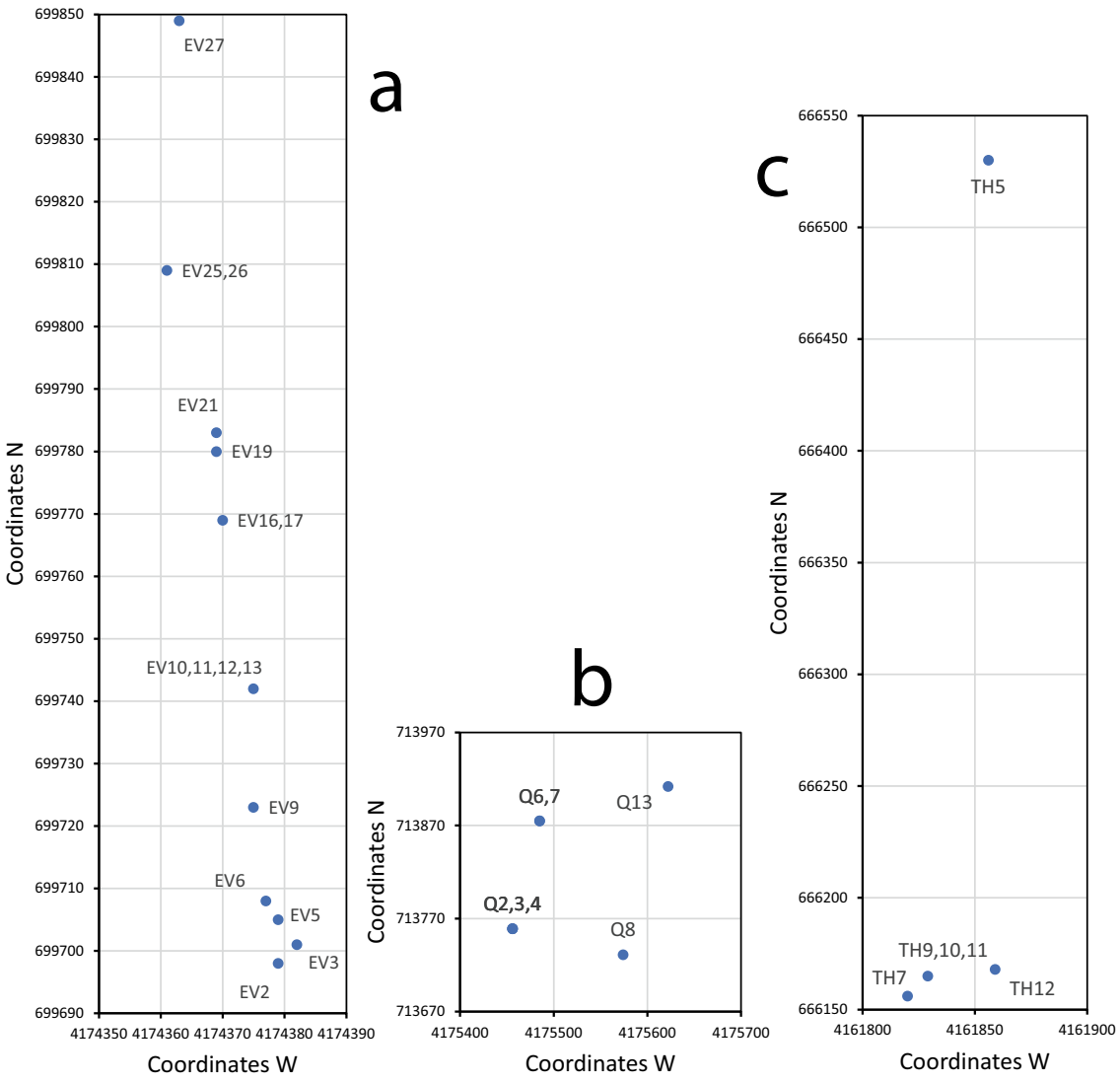

Fig. 1. Locations of the sampled specimens (GPS coordinates) to provide the relative position of the samples within each site. Within each plot, north (N) and west (W) coordinates have the same lateral dimensions. However, coordinate dimensions vary from plot to plot. (a) El Villar, which represents a N-S section of ~20 m; (b) Quebrantahuesos, where collection points are in the approximate range 15–30 m; (c) Tharsis, where the *E*-W section at the bottom is ~10 m. Calañas is not shown because there are only two samples collected several meters apart.

carried out with Cu Kα radiation, at 45 kV and 40 mA, using a Ge monochromator, a divergence slit of 0.25° and Soller 1 and 2 slits of 1.146°. This apparatus uses a solid-state detector (X'Celerator) that covers an angle of 2.1° and dynamically integrates the diffracted intensity over that angle as it scans. The samples were scanned in the range 2–80°2θ, with a resolution of 0.0167°2θ (scan step in a conventional scanner), and the total collection time was 60 min (equivalent to 0.77 s/step).

The <2 μm fractions were also analyzed as oriented mounts, to investigate in detail the clay mineralogy and their relative proportions. They were studied as air-dry and as treated with ethylene-glycol (EG) by overnight solvation in an EG-saturated atmosphere at 60 °C. The XRD scan range was 2–40°2θ, with a scan duration of 63 min (equivalent to 1.66 s/step). All other conditions were the same as described above. The corresponding XRD patterns were simulated using ClaySIM from MDI, which uses the Newmod code (Moore and Reynolds Jr., 1997). This tool allows calculation of the relative proportion of phyllosilicate minerals present, whether end-member or interstratified phases, excluding all other minerals present. For further information see Mavris et al. (2018).

3.2.2. *REE analysis*

Trace and REE concentrations were analyzed from whole-rock fractions in the same sample processing in which the major element compositions were determined (Mavris et al., 2018). The samples were kept in a desiccator at room temperature prior to analysis after drying at 107 °C for a minimum of 12 h. REE were analyzed by inductively coupled mass spectrometry (ICP-MS) using an Agilent 7700× instrument after acid digestion. Samples (50 mg) were treated with 4 ml HF, 1 ml HNO_3 and 2 ml $HClO_4$ (trace metal analysis grade) in closed 60 ml fluoropolymer vessels (Savillex™) at 100 °C for 48 h, after which the resulting solutions were evaporated to dryness at 150 °C, treated with further 1 ml portion of $HClO_4$, evaporated again, re-dissolved in 2 ml of HNO_3 and made up to 50 ml with Milli-Q water. Concentrations were determined using gravimetrically prepared REE standard solutions for calibration. The stability of the measurement sessions was monitored by repeat analyses of the REE standards at regular intervals and, where necessary, used to correct for any instrumental drift. Accuracy was controlled by the analysis of the certified reference material BCR-2 (Basalt, US Geological Survey), and the analytical error ranged 9.7–0.10% of the ppm concentrations of the analyzed elements. REE concentration values are provided in Table S1.

The REE concentrations were normalized with respect to the average upper crust composition (Table 5 of McLennan, 2001), which McLennan (2001) estimates a more accurate or informative normalization than those with respect to NASC or PAAS. Principal component analysis (PCA) of mineralogical and REE composition variables was carried out to investigate how minerals modified the REE signature. The variables had heterogeneous values and the mineral concentrations were estimated in different ways. The phyllosilicates were divided in two variables, the relative concentration of those formed hydrothermally before the acid alteration (original clays) and those formed by action of the acid alteration. Their proportions were obtained from the simulation of XRD patterns of oriented mounts of the <2 μm size fraction, where the phyllosilicates were abundant. In most cases, only quartz was more abundant than phyllosilicates in the bulk rock (see below) but quartz contribution to REE composition is negligible in this type of rocks (McLennan, 2001) and can be ignored. As phyllosilicates were abundant in most bulk-rock samples and phyllosilicates concentrate REE in alteration environments (McLennan, 1989) their relative proportions from the <2 μm size fraction was assumed to be a good approximation to the mineralogical influence on REE distribution in the samples. In the cases where phyllosilicate contents in the whole rock were low (samples EV9, 16, 17, 19, Q4, TH5 and TH9) the proportion of phyllosilicates (from the <2 μm size fraction) was multiplied by a factor that ranged from 0.05 to 0.3. These factors were estimated by comparing the relative intensity of the most intense XRD peak of quartz (3.34 Å) to the most intense phyllosilicate peak. In summary, the concentration of phyllosilicates used in the PCA analysis (taken from the <2 μm size fraction) is an accurate representation of the relative proportion of original phyllosilicates and those formed from acid alteration, but it is only an approximation of the absolute proportion of phyllosilicates versus other minerals, where corrections were performed only in cases where phyllosilicate contribution to the whole fraction was estimated as ≤30 wt%.

The individual proportions of the other minerals, except goethite, were assessed assigning the values 0, 20, 40 or 60 wt%, depending on the relative intensities of their most intense peaks in the whole rock. For the PCA, the contents of alunite and jarosite were added together and correspond to the variable termed sulfate abundance. Plagioclase and feldspar were assessed together and added to quartz. Tests of the PCA analyses separating or adding together quartz and plagioclase/feldspar showed in both cases that their corresponding vectors exactly aligned, for which reason it was resolved to use the variable quartz + plagioclase/feldspar, for simplicity. The proportion of goethite was calculated from thermogravimetric analysis of the whole rocks (Cuadros et al., 2020).

The variables corresponding to the REE used in the PCA were slope, calculated as the ratio La/Lu, Eu anomaly, calculated as $([Sm \times Gd]^{0.5} / Eu)$, Ce anomaly, as $(La + Pr)/(2 \times Ce)$, and average content of REE ([ΣREE]/n; where n is the number of values). Because the range of values for the Eu anomaly, Ce anomaly and average REE content were much narrower than those of the other variables, the corresponding values were multiplied by a factor of 10, which increased their range of variation and allowed these three variables to have a weight similar to all the others.

4. Results

4.1. XRD results

The results of powder XRD analysis of the bulk rocks are displayed in Table 1. Samples EV2, QX and TH12 are the original rock in each of the corresponding sites; i.e., the rock unaffected by acid alteration. Calañas (C) does not have an unaltered representative. In Calañas, illite and quartz appear to be the main components of the rock subjected to the acidic alteration, although chlorite may have also been present (Mavris et al., 2018). Sample C2 is more altered than C1, as indicated by the presence of kaolinite in the former. In El Villar (EV), the rock previous to the acidic alteration consisted of quartz, illite, chlorite and plagioclase/feldspar (Table 1). The acid alteration was mild although generally intensifying from samples EV3 to EV25. In the least altered specimens, chlorite was slightly weathered (wide chlorite XRD peaks), while increasing alteration caused its complete weathering to kaolinite. Plagioclase/feldspar and, to a lesser extent, illite also generally decreased as kaolinite proportion increased (Table 1). In Quebrantahuesos (Q), the rock that underwent acidic alteration (sample QX) consists mainly of quartz and chlorite (Table 1). The alteration of these rocks was substantial, producing mineral phases associated with a pH range 5 to <3, such as alunite (pH 5–3) and beudantite-jarosite (pH < 3). In Tharsis (TH), the unaltered sample from the initial shales consists of quartz, illite and kaolinite. Its acidic alteration covered a range of pH similar to that of Q samples, as demonstrated by the existence of alunite and jarosite, although the greater abundance of jarosite in Tharsis indicates that strongly acidic fluids (pH < 3) were more frequent (Table 1). No phosphate minerals were detected in any sample. Their possible influence in REE concentration in this study is discussed in section 5.1.

Table 1
Mineralogy of bulk-rock samples from XRD.

Sample	Mineralogy	Sample	Mineralogy
C1	Qz, Illite	EV26	Qz > Plg/Fds > Goethite
C2	Qz, Illite > Kaolinite	EV27	Qz > > Plg/Fds
EV2[1]	Qz > Illite, Chlorite > Plg/Fds	QX[1]	Qz, Chorite
EV3	Qz > Illite, Chlorite > Plg/Fds	Q2	Qz, Alunite
EV5	Qz, Illite, Chlorite (w), Plg/Fds	Q3	Qz, Alunite
EV6	Qz > > Illite, Chlorite (w), Kaolinite, Plg/Fds	Q4	Qz, Alunite > > Illite
EV9	Qz > Plg/Fds > Kaolinite	Q6	Qz, Illite > Alunite > Hematite
EV10	Qz > > Kaolinite, Plg/Fds >> > Illite	Q7	Qz > Illite, Alunite
EV11	Qz > Illite, Kaolinite, Plg/Fds	Q8	Beudantite[2] > Qz, Illite, Goethite
EV12	Qz > Illite, Kaolinite, Plg/Fds	Q13	Qz > > Goethite
EV13	Qz > Illite, Plg/Fds > Kaolinite	TH12[1]	Qz, Illite, Kaolinite
EV16	Qz > Plg/Fds >> > Illite	TH5	Qz, Goethite > > Kaolinite
EV17	Qz > Kaolinite > Illite, Plg/Fds	TH7	Qz, Illite, Alunite > Kaolinite > Goethite
EV19	Qz > Plg/Fds > Illite, Kaolinite	TH9	Qz > Goethite > Jarosite
EV21	Qz > Plg/Fds	TH10	Jarosite > Qz
EV25	Illite > Qz	TH11	Qz, Jarosite

Qz: quartz; Plg/Fds: plagioclase/feldspar. Minerals separated by commas have comparable concentrations.
w: With signs of weathering.
[1] Rocks not altered by acidic fluids.
[2] Contains some jarosite.

4.2. Normalized REE concentrations

The REE patterns of the C samples are approximately flat (Fig. 2). Both have Ce and Eu negative anomalies. Sample C2, which has a higher level of acidic alteration, is slightly depleted of REE with respect to C1. HREE in C2 are slightly depleted relative to the rest of REE.

EV samples have rather similar REE patterns with a few exceptions (Fig. 3). Most of them follow approximately the pattern of sample EV2, which is the rock untouched by acidic alteration. This pattern consists of a slightly higher concentration of HREE over LREE, a shallow negative Ce anomaly and a deep Eu anomaly. Normalized REE average concentrations within samples (average REE concentration of each sample) vary between ~0.7 and ~ 5. Most samples are depleted in REE with respect to sample EV2, with only EV13, EV5 and EV12 showing REE enrichment (in decreasing order). The most important modifications to the REE pattern of EV2, apart from absolute REE concentrations, are the following.

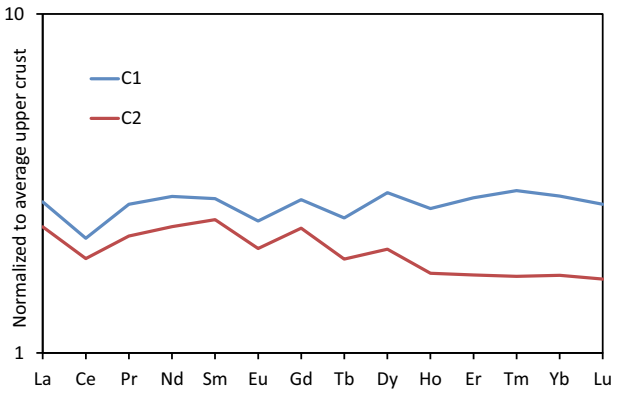

Fig. 2. REE concentrations in the samples from Calañas.

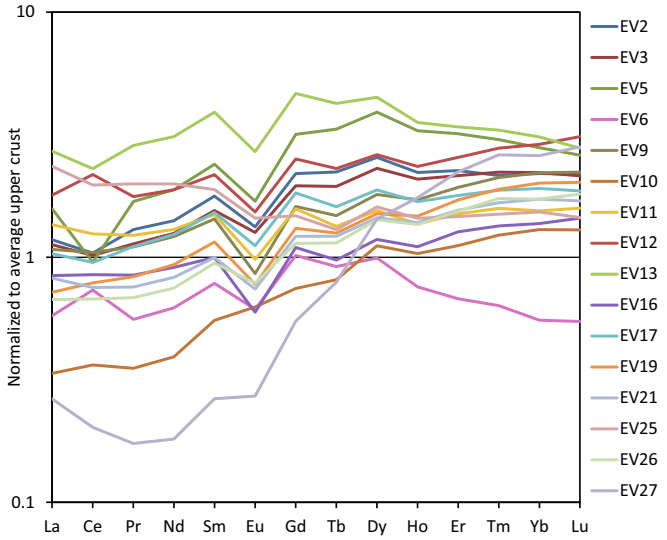

Fig. 3. REE concentrations in the samples from El Villar. EV2 was not altered by acidic fluids.

Sample EV27 is strongly depleted of LREE as compared to HREE but preserves a negative Eu anomaly. The most obvious mineralogical difference of this sample with respect to the rest is that it contains a very little proportion of phyllosilicates. None was detected in the whole fraction using XRD (Table 1) but XRD and IR investigation of the <2 μm fraction revealed illite traces (Mavris et al., 2018). Sample EV27 is dominated by quartz with some plagioclase/feldspar (Table 1). Sample EV10 has a similar but less pronounced REE pattern shape. Interestingly, this sample does not display Eu anomaly. The mineralogy of EV10 is also dominated by quartz, with lower concentration of kaolinite and plagioclase/feldspar, and with traces of illite (Table 1). However, EV21 is also dominated by quartz and plagioclase/feldspar (Table 1) while not displaying a substantially different REE pattern from that of EV2 (Fig. 3).

One more modification of the REE pattern with respect to that of EV2 that appears in several samples is a slight depletion in HREE which, together with the Eu anomaly, imprints something of an "M" shape to the patterns. This modification is clear in samples EV13 and EV5, the two with the highest REE concentrations, and in EV6, one of the samples with lowest average REE concentration (Fig. 3). There is no obvious mineralogical characteristic that links these samples or distinguishes them from the rest (Table 1). There is one more important modification of the REE patterns that involves the above samples and others next to them in the sampled rock. Samples EV12 and EV6 have clear positive Ce anomalies. Sample EV5, neighbour of EV6 (Fig. 1), has a deep negative Ce anomaly. Sample EV13, neighbour of EV12, has a negative Ce anomaly somewhat deeper than that of the original rock (EV2). This suggests some process linking the Ce concentrations of EV5 and EV6 on the one hand and of EV12 and EV13 on the other. Adjacent to the latter two specimens (Fig. 1), sample EV10 has also a shallow positive Ce anomaly and EV11 a shallow negative Ce anomaly.

Quebrantahuesos and Tharsis are the two sites where acidic alteration was intense, with pH $\leq$ 5 (Mavris et al., 2018), which is reflected in that the range of REE concentrations is wider than in the two other sites (Figs. 2-5), due to intense processes of concentration and dilution of REE. In Quebrantahuesos, the original rock (QX), containing major quartz and chlorite, had an REE signature similar to the original rock from El Villar (EV2). There is in both a gentle positive slope from LREE to HREE and a negative Eu anomaly (Figs. 3 and 4). However, there is no Ce anomaly in QX (Fig. 4). Sample Q13, consisting of major quartz and minor goethite, has an almost identical signature, with the important modification of a positive Eu anomaly. Samples Q6 and Q7 have approximately similar patters to QX but with no Eu anomaly and more flat concentration patterns. Sample Q8 contains major beudantite (Table 1). The overall REE pattern of Q8 is similar to that of the original rock, but with higher concentration. The largest modification to the REE patterns occurs in samples Q2, Q3 and Q4, all three containing major alunite and quartz (Table 1). In these samples the LREE have been largely concentrated and the HREE depleted to a lesser extent, in comparison with QX. The resulting REE pattern is frequent, in the main lines if not in every detail, in sulfates and particularly alunite (e.g., He et al., 2006; Kikawada et al., 2013).

The original rock from Tharsis (TH12) had a flat REE pattern, with a positive Eu anomaly (Fig. 5). This sample consists of hydrothermal illite and kaolinite. The pattern is similar for samples TH7 and TH9, although they have higher and lower REE concentrations than TH12, respectively. Samples TH7 and TH9 do not have similar mineralogy (Table 1). Sample TH5 has a flat REE pattern, with no Eu anomaly and a slight depletion of HREE. This sample consists of quartz, goethite and minor kaolinite (Table 1). Finally, samples TH10 and TH11 are enriched in LREE and depleted of HREE with a positive Eu anomaly. Both consist of jarosite and quartz (Table 1).

4.3. Discrimination between silicate- and sulfate-rich rocks

In a general overview of the REE patterns of all samples, it is suggested that those consisting of silicates, both tecto- and phyllosilicates,

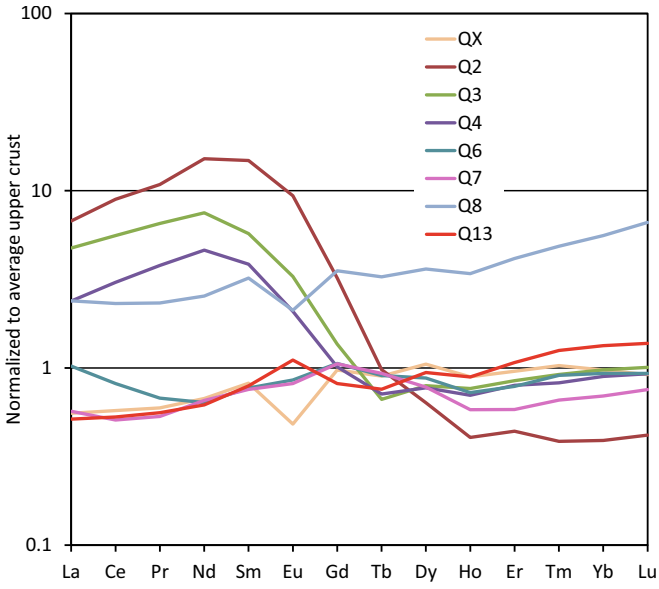

Fig. 4. REE concentrations in the samples from Quebrantahuesos. QX was not altered by acidic fluids.

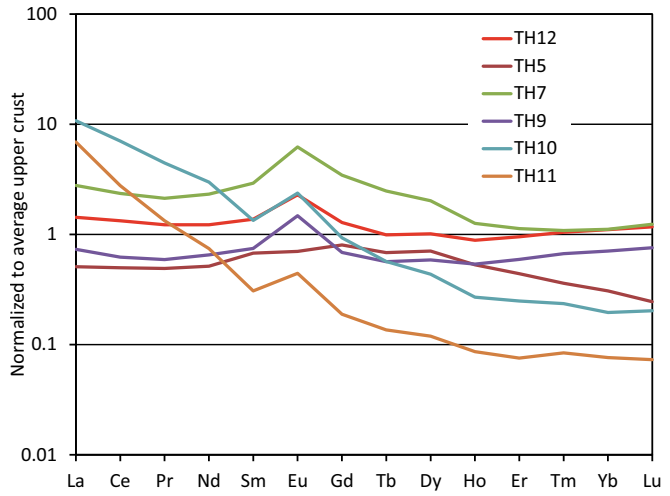

Fig. 5. REE concentrations in the samples from Tharsis. TH12 was not altered by acidic fluids.

are generally characterized by flat or little-skewed REE patterns and/or by a negative Eu anomaly. Conversely, samples with major sulfates frequently do not have Eu anomaly and/or have REE patterns with substantially higher concentrations of LREE than of HREE. It was then investigated whether using these two parameters could produce plots capable to discriminate silicates from sulfates. The Eu anomaly was represented as.

$(Sm_N \times Gd_N)^{0.5} / Eu_N$, the inverse of the usual value ($Eu/Eu^* = Eu_N / [Sm_N \times Gd_N]^{0.5}$; McLennan, 1989) because the inverse values of a negative Eu anomaly are >1 and allow a more clear graphical representation.

The results indicate that this discrimination is possible, although there is no gap between the two groups of samples (Fig. 6). Samples with REE patterns dominated by silicates are mostly those that underwent mild acidic alteration. They are all the EV and C samples, at the right of the grey line, with EV10 and EV25 right next to this line (Fig. 6). Samples with REE patterns dominated by sulfates and goethite are those that underwent strong acidic alteration, resulting in (1) abundant sulfates and/or goethite and/or (2) destruction or large reduction of

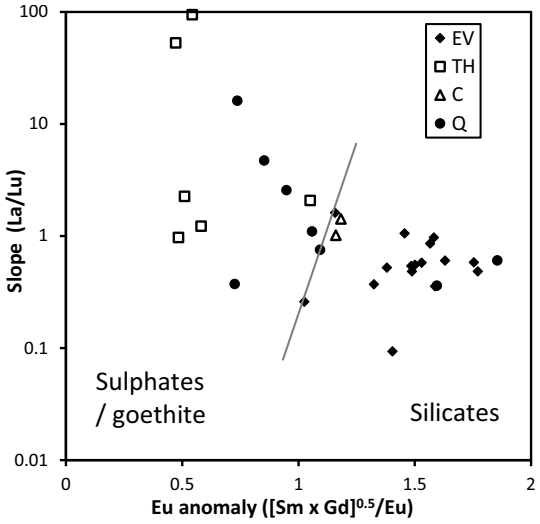

Fig. 6. Magnitude of the Eu anomaly versus the slope of the REE patterns as represented by the ratio La/Lu. The Eu anomaly is here calculated as the inverse of the usual value (see text). The plot allows the discrimination of samples where REE are controlled by silicates from those where REE are controlled by sulfates and/or goethite (but see further discussion about goethite in the text).

silicates except quartz. These samples appear at the left of the line (Fig. 6). Two Q samples are to the right of the grey line, QX (far right), which is the unaltered rock (Table 1) and Q8, which had abundant beudantite (Table 1) and was located below and close to the pyrite body that produced the acidic fluids. Q7 is on the line, a sample containing major quartz, illite and alunite (Table 1).

The average concentration of REE might have been also a discriminatory factor between the two groups of samples, as it appears to be higher in those subjected to intense acidic alteration (Figs. 2-5). However, plots incorporating this variable (not shown) were less discriminatory than the plot in Fig. 6.

4.4. PCA analysis

In order to integrate all variables in a single analysis of the behavior of REE, PCA analysis was carried out. The difficulty with the data is that they are heterogeneous, with different units and where some are truly quantitative but some are assessed data. The elaboration of the data to allow a PCA with sufficient resolution is explained in the methods and the values are displayed in Table S2.

The PCA analysis shows that 54.3% of the variance of the data is explained by component 1, and 24.7% of the variance by component 2. The Eu anomaly is linked to the proportion of acid-altered phyllosilicates and, to a lesser extent, to the proportion of quartz plus plagioclase/feldspar (Fig. 7). Interestingly, the Eu anomaly is not linked to the proportion of the original phyllosilicates (of hydrothermal origin, rather than produced by acidic alteration). This may be a partial artifact of the fact that original phyllosilicates and those product of alteration are inversely correlated (the phyllosilicates product of alteration were formed mainly from the original ones). This result may also be influenced by the fact that the TH samples have a positive Eu anomaly and some of them preserve significant amounts of original phyllosilicates. In any case, it indicates that the Eu anomaly is more developed in the

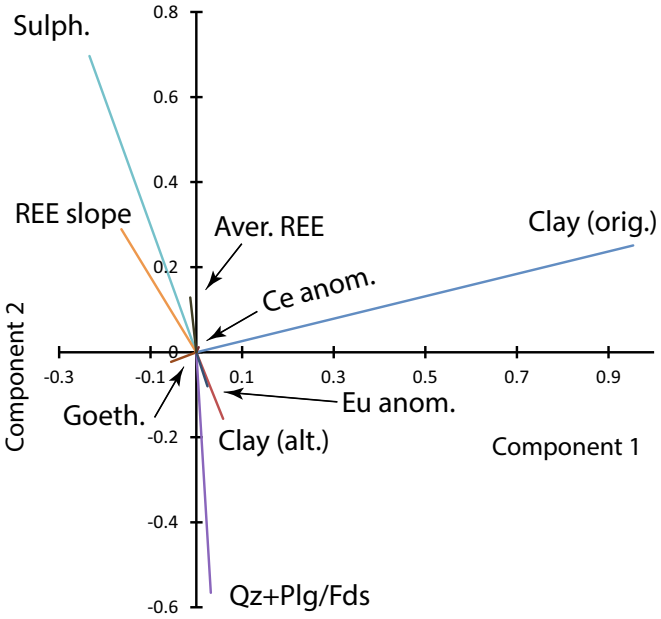

Fig. 7. Principal components analysis (PCA) of mineralogical and REE-related variables of the investigated samples. The plot with the two main components establishes which variables are mutually related by their proximity in the plot. Clay (orig.): proportion of original phyllosilicates of hydrothermal origin; Clay (alt.): proportion of phyllosilicates product of acidic alteration; Qz + Plg/Fds: assessment of proportion of quartz plus plagioclase/feldspar; Goeth.: proportion of goethite; Sulph.: assessment of proportion of sulfates; REE slope: La/Lu ratio; Aver. REE: average concentration of REE; Ce anom.: Ce anomaly values; Eu anom.: Eu anomaly values.

phyllosilicates product of alteration than in the original ones. The Ce anomaly vector has a very small length in the plane of Fig. 7 and shows little connection with mineralogical variables. The slope of the REE patterns and, to a lesser extent, the average REE concentration are both mainly linked to the proportion of sulfates in the samples. Goethite proportion is not linked to Eu negative anomaly (angle between vectors ~90°; Fig. 7), and very weakly linked to the REE slope (positively) and average REE concentration (negatively, as the corresponding vector angles are a little below and above 90°, respectively; Fig. 7). The above results seem to contradict those from Fig. 6, where goethite appears associated with the sulfates when considering the Eu anomaly and REE slope. However, there is an important difference between Figs. 6 and 7. The distribution of mineral phases in Fig. 6 considered major minerals only, based on XRD results, whereas the PCA used quantitative goethite contents from thermogravimetric data (see methods), which in many cases were in low concentration and not detected with XRD (Table 1, Fig. 6). In any case, the PCA data show that the variable most positively correlated to goethite content is the REE slope, itself highly correlated to sulfate content (Fig. 7).

The above results can be investigated more in detail considering the correlations of the individual variables with the scores of the PCA for each of the two main components (Fig. 8). The most clear link between a mineralogical and REE variable is that of sulfates and REE slope, which

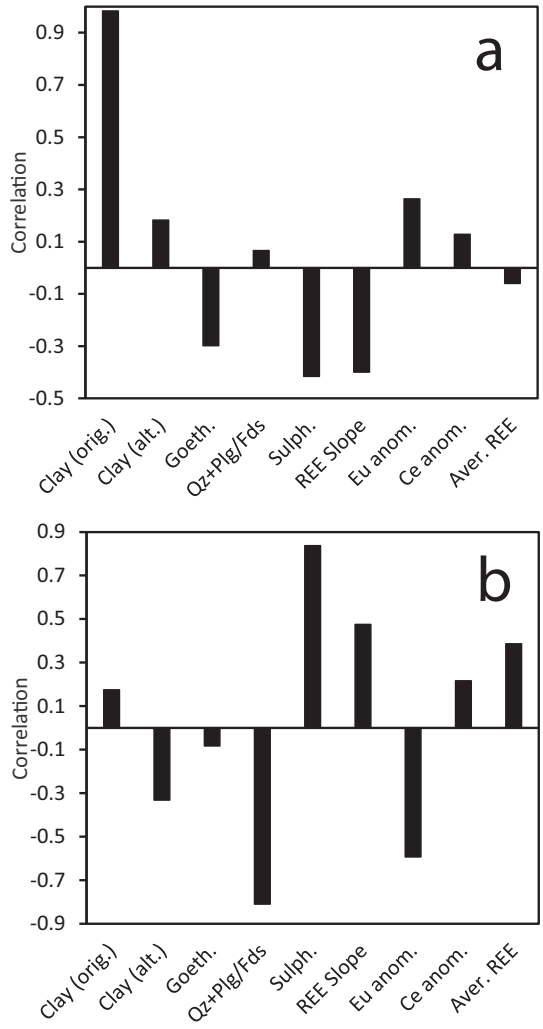

Fig. 8. Correlation between the scores of the principal component analysis (PCA) and each individual variable, for the first (a) and second (b) components. Variables with high correlation values of the same sign are correlated to each other.

two variables display significant correlation values of the same sign within both components. The Eu anomaly has opposite correlations with original phyllosilicates and with goethite in components 1 and 2, whereas the correlation is positive for both components with phyllosilicates produced by acidic alteration and with quartz plus plagioclase/feldspar. The average REE concentration is significantly linked only to the proportion of sulfates, and this only in component 2 (Fig. 8b). The Ce anomaly has very weak links to mineralogical variables. The development of the negative Eu anomaly is negatively correlated to the slope of REE patterns and less so to the average REE concentrations for both components. This negative correlation allows the discrimination between samples with REE signature dominated by silicates (negative Eu anomaly) and those dominated by sulfates (steep slope of REE patterns) (Fig. 6).

5. Discussion

5.1. Possible role of phosphates in shaping REE signature

The possible role of phosphates in controlling the concentration and segregation of REE in our samples was tested. Although no phosphate minerals were detected with XRD in any of the samples, amounts below their XRD detection level could exercise such control. The test used measured amounts of P in the samples. Lack of sufficient P to contain all REE within most samples, lack of correlation between P and REE contents, and evidence that P was present within other mineral phases, rather than only as phosphates, all indicate that phosphates were not controlling REE modification by acid alteration (Table S3, Fig. S2 and corresponding discussion in the Supplementary material).

5.2. REE signature of the rocks previous to acidic alteration

Although the four sites investigated have distinct REE features resulting from the acid alteration process, the original rocks have similarities (Fig. 9). Samples EV2 and QX have a clear negative Eu anomaly and a small positive slope from LREE to HREE. Differences are the slightly higher concentrations in EV2 and the presence of a shallow negative Ce anomaly in EV2, absent in QX. There is no original rock sampled in Calañas but the least altered of the two samples has REE patterns resembling those of EV2, i.e., similar REE concentrations and negative Ce and Eu anomalies. Differences are the relative depths of the Ce and Eu anomalies and skewness of the REE patterns. From these data, it can be concluded that the nature of the rocks before the acid alteration

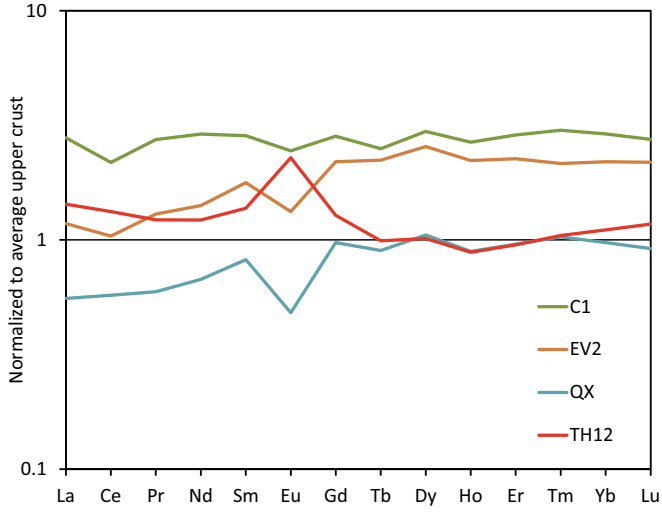

Fig. 9. REE concentrations in the samples that were not altered with acidic fluids (EV2, QX, TH12) or with the lowest alteration (C1), from each of the investigated sites.

in Calañas, El Villar and Quebrantahuesos as well as the processes generating them were approximately similar, of volcanic type. Such conclusion is corroborated by previous work. The original rock in El Villar was produced by hydrothermal alteration of basalts with minor rhyolites and dacites (Mavris et al., 2018). In Calañas, the original rock was produced by hydrothermal alteration of acidic tuffs (Mavris et al., 2018). In Quebrantahuesos, the hydrothermal alteration took place on felsic porphyritic volcanics (Adamides, 2013).

On the contrary, the REE patterns of the original rock from Tharsis, TH12, is different from the rest of the original rocks. Sample TH12 is slightly enriched in the HREE Er to Lu, has a clear positive Eu anomaly and no Ce anomaly (Fig. 9). REE concentrations, however, are similar and intermediate between those of Quebrantahuesos and the other two localities. The original rock was generated by the hydrothermal alteration of shales with minor felsic volcanics, hosting stockwork-like and small lenticular sulfide masses (Tornos, 2006; Tornos et al., 2008). These small sulfide veins and lenticular sulfide masses are previous to the formation of the large tonnage massive sulfide bodies and their associated hydrothermal alteration (Tornos et al., 2008).

The most probable interpretation of the positive Eu anomaly in the samples from Tharsis is that it is a signature of the shales that were deposited between the Late Famennian (~360 Ma) to the Early-Late Visean (~335 Ma; Tornos, 2006). These are the shales that, together with minor felsic volcanics and small veins and lenticular masses of sulfides were hydrothermally altered to quartz, kaolinite and illite during the emplacement of the massive sulfide orebody contemporaneous to their sedimentation (Tornos, 2006; Toscano et al., 2014). The most immediate interpretation of a positive Eu anomaly is an enrichment in plagioclase (McLennan, 1989) either in the sedimented shales, if plagioclase preservation was possible, or in the precursor of the shale. In the latter case, the shales would have retained the high Eu concentration from their precursor. Interestingly, hydrothermal alteration during massive sulfide emplacement produced major kaolinite (Table 1, sample TH12), a typical product of hydrothermal alteration of feldspar-plagioclase, although this is not proof that plagioclase was abundant in the shale. Whatever the particulars of the case, this interpretation is coherent with Tharsis having the only precursor rock from the studied sites with a positive Eu anomaly (Fig. 9) because of its different origin. The precursor rocks in El Villar, Calañas and Quebrantahuesos were all volcanics of different composition deposited around the time of hydrothermal alteration, whereas most of the material from Tharsis were shales.

5.3. General trends of REE patterns produced by acidic alteration

The concentrations of REE normalized to average crust composition are variable in all sites, including important variations in the mildly altered El Villar (pH 5–7), which indicates complex controls on this variable. After the initial hydrothermal alteration, the range of normalized concentrations is 0.5 in QX to 3 in C1 (Fig. 9), whereas after acidic alteration, the range increases to that from 0.07 in TH11 (Fig. 5) to 15 in Q2 (Fig. 4).

The common modifications of REE patterns produced by acidic alteration across localities are considered first (Figs. 7 and 8) while specific behavior within localities will be discussed below. Visual inspection of the REE patterns (Figs. 2-5) contrasted with sample mineralogy (Table 1) indicates that mild acidic alteration (pH 5–7; Mavris et al., 2018), where sulfates did not form, and where the final mineral suit consisted of silicates (inherited quartz, plagioclase/feldspar, illite and chlorite, together with neoformed kaolinite; Table 1), preserved largely the shape of the REE patterns of the original rock, although there were modifications to the concentrations. The above mineralogical information was obtained from XRD of the whole rock (Table 1). Investigation of the <2 μm size fraction completed the above mineralogical description indicating the existence of interstratified chlorite-vermiculite, illite-smectite and kaolinite-smectite, as well as minor vermiculite (Mavris et al., 2018). Because quartz contains low REE levels while phyllosilicates (and potentially plagioclase in EV) have high concentrations (e.g., McLennan, 1989; Borst et al., 2020), the conservative REE behavior indicated above is interpreted as a preservation of the REE signature of the pre-existing phyllosilicates (and plagioclase/feldspar in EV) in the subsequent phyllosilicate mineral suit generated by acidic alteration. The mildly acidic pH of the fluids very likely produced progressive mineral changes where REE were not released in bulk into the fluids but rather bonded to the crystallizing phyllosilicates, which offered more and stronger binding sites than the fluids. These conditions would also reduce the capacity of phyllosilicates to segregate REE. This interpretation is in line with the low capacity of circa-neutral fluids to modify REE patterns in rocks and the limited REE segregation of REE by phyllosilicates (McLennan, 1989; Prudêncio et al., 1989).

Interestingly, almost all EV samples have a negative Eu anomaly even though most of them contain plagioclase/feldspar, which usually concentrates Eu (McLennan, 1989). This is consistent with the previous finding that most volcanic rocks emplaced across a wide area of the Iberian Pyrite Belt display a negative Eu anomaly (Mitjavila et al., 1997). Accordingly, the plagioclase in the El Villar volcanic protolith (before the hydrothermal process emplacing pyrite) did not have a high Eu concentration. It is possible to corroborate that plagioclase/feldspar in El Villar has a negative Eu anomaly by investigating the REE patterns of samples in our study where plagioclase/feldspar is much more abundant than phyllosilicates and thus it is expected that the measured REE signature is that of plagioclase/feldspar. Four cases exist: EV16, EV25, EV26 and EV27 (Table 1), all with a negative Eu anomaly, from deep (EV16) to very shallow (EV25) (Fig. 3). It can be concluded that the negative Eu anomaly in El Villar is inherited from the volcanic protolith.

The intense acidic alteration produced precipitation of alunite (pH 3–5) and jarosite (pH < 3; Mavris et al., 2018), as well as goethite. The latter may have formed during acidic alteration at pH 3–5 or as weathering of jarosite at a later stage (Mavris et al., 2018). Formation of sulfates produced three changes in the REE patterns: enrichment of LREE with respect to HREE (represented as REE slope in Figs. 7 and 8), increase of average REE concentration, and enrichment of Eu (Figs. 7 and 8) manifested in a range of situations from shallow negative to positive Eu anomalies (Fig. 4). However, the positive Eu anomaly in Tharsis is inherited from the shale protolith rather than the product of acidic alteration (Fig. 5). Enrichment of LREE with respect to HREE has been reported before for sulfates precipitated from acidic fluids altering silicates both at low temperature and in magmatic or hydrothermal systems, including gypsum (Inguaggiato et al., 2020), alunite (Terekado and Fujitani, 1998; Deyell et al., 2005; Martínez et al., 2006; He et al., 2006; Parsapoor et al., 2009; Kikawada et al., 2013; Inguaggiato et al., 2017; Ondrejka et al., 2018) and jarosite (Parsapoor et al., 2009; Welch et al., 2009). In one case, alunite displayed also a prominent positive Eu anomaly (Deyell et al., 2005). Other reports, however, indicate that acid-altered rocks containing jarosite, beudantite or similar phases frequently preserve the REE patterns of the original rocks. Leybourne et al. (2006) asserted that gossans with jarosite-group minerals and beudantite typically preserve REE patterns of the previous rock, although there are occasional cases in which the pattern is altered to display LREE > HREE. Romero et al. (2010) reported that original rock and acid-altered mine sediment (with Pb-bearing barite, beudantite, Fe-oxyhydroxides, jarosite, anglesite and plumbojarosite) showed little variation of REE patterns. Mitra et al. (2017) found no REE pattern differences between jarosite and the surrounding shale. Similarly, Pérez-López et al. (2010) reported little REE pattern modification from sulfide orebody (rather than silicate rock) to gossan (70–85% quartz, 5–10% hematite, 1–5% goethite, 1–5% jarosite, 1–5% beudantite and minor micas) in the São Domingos mining district (Iberian Pyrite Belt, but not coincident with the areas investigated in the present study). In summary, judging from the frequency of findings of alunite or jarosite with LREE > HREE, it appears that this REE segregation is stronger or more effective in alunite than jarosite.

In samples from the present study where alunite and/or jarosite dominated mineralogy (without considering quartz, where REE concentrations are low) there was an obvious pattern of LREE > > HREE (samples Q2, Q3, Q4, TH10, TH11; Table 1, Fig. 10a), although with different specific shape in alunite- and jarosite-dominated samples. This is not the case of the sample dominated by beudantite (Q8, Fig. 4, Table 1), which exactly mimics the original rock (QX, Fig. 4). Because there is illite and goethite in this latter sample, which may have controlled REE signature, the following discussion is focussed on samples Q2, Q3, Q4, TH10 and TH11, where the sulfate phases are the only control. One possible reason for the pattern of LREE > > HREE is REE segregation produced by complexing agents in solution. At pH below 7 in sulfuric fluids, two are the most abundant types of REE species, the ionic Ln^{3+} species (where Ln represents lanthanide) and complexes with SO_4^{2-} anions, where the latter become more abundant as the pH decreases (Gimeno-Serrano et al., 2000; Welch et al., 2009 and references therein; Ayora et al., 2015). The equilibrium constants of the two main aqueous sulfate complexes ($LnSO_4^+$ and $Ln[SO_4]_2^-$) are similar for all REE (Brookins, 1989; Gimeno-Serrano et al., 2000; Schijf and Byrne, 2004), which means they cannot cause segregation between solution and solid phases (Gimeno-Serrano et al., 2000). Neither can the individual ionic Ln^{3+} species. Consequently, the acidic, sulfate-dominated fluids that altered the rocks in Quebrantahuesos and Tharsis were unable to segregate REE contrary to what was observed in alunite and jarosite (Fig. 10a).

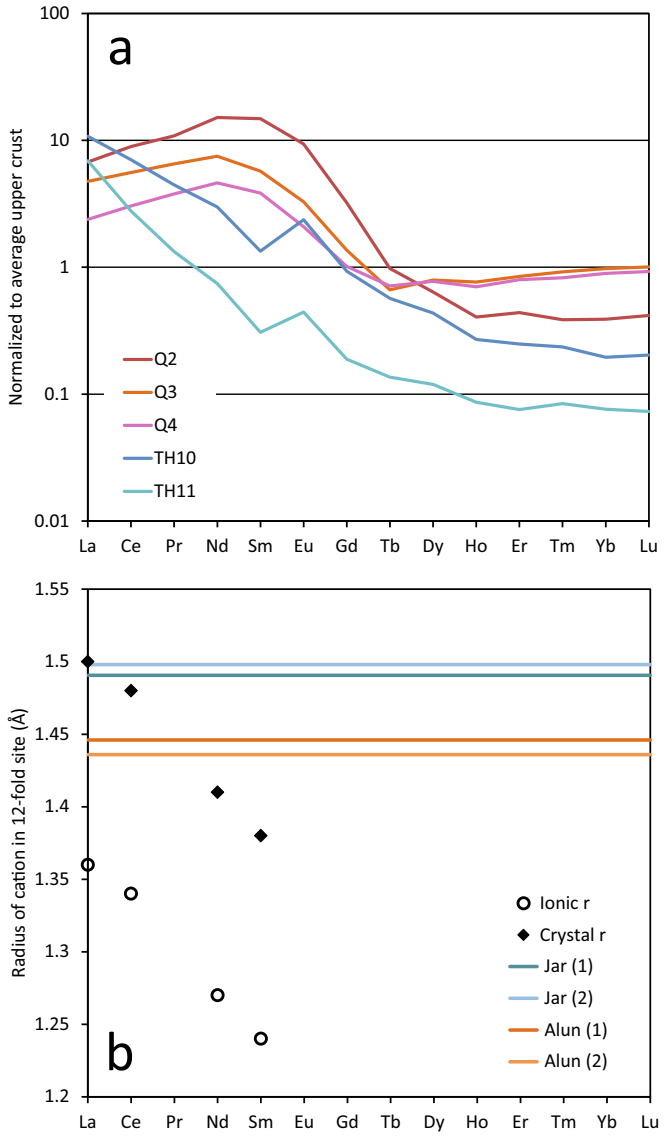

Fig. 10. (a) REE signatures from samples entirely dominated by alunite (Q2, Q3, Q4) and jarosite (TH10, TH11). (b) Calculated radii of some lanthanides of charge 3+ in 12-fold coordination (data points; from Shannon, 1976) and experimental radius of K^+ in 12-fold coordination in jarosite and alunite, from (1) Kato and Miura (1977) and (2) Sato et al. (2009). The calculated lanthanide radii correspond to the ionic (hollow circles) and crystal (full diamonds) values. No values are available for REE beyond Sm^{3+} but radii should decrease monotonously towards Lu^{+3}.

The cause of REE segregation may be preferential scavenging from solution by alunite and jarosite. Such an effect is strongly suggested by the following study. Dutrizac (2017) precipitated gypsum in controlled conditions (pH 3.0, 75 °C) in the presence of REE in a wide range of concentration (1–5 g/l). In most experiments the solutions were dominated by sulfate anions, with chloride present in a wide range of concentrations ($[Cl^-]$ / $[SO_4^{2-}]$ ranged approximately 0.1–1). Thus, chloride was an important component in some of the experimental fluids. However, as the stability constants of Ln^{3+} complexes with chloride ions are orders of magnitude lower than those with sulfate, REE speciation in these fluids must have been controlled by sulfate complexes and free Ln^{3+} species. Dutrizac (2017) found that REE concentration in the precipitated gypsum (1) was always higher for LREE than HREE, as in our samples in Fig. 10a, and (2) had the maximum at Pr—Nd, similarly to our alunite samples (maximum in the range Nd—Sm, Fig. 10a). Dutrizac (2017) found that REE always substituted for Ca in gypsum, i.e., 3 Ca^{2+} ions were substituted by 2 Ln^{3+} plus a vacant site. Dutrizac pointed out that the ionic radii of LREE are more similar to that of Ca^{2+} than are those of HREE. This author concluded that the size of the crystallographic site occupied by the REE controlled their relative proportion in gypsum.

We explored the possible sites where REE may be lodged in jarosite and alunite. The Fe^{3+} or Al^{3+} octahedral sites would be ideal from the perspective of electric charge as no change would result. However, the ionic radii of octahedral Fe^{3+} and Al^{3+} are 0.65 and 0.54 Å (Shannon, 1976), much smaller than those of the Ln^{3+}, which range from 1.03 Å, for La, to 0.86 Å for Lu. Moreover, according to these values, HREE should be preferentially retained in octahedral sites because their ionic radii are most similar to those of Fe^{3+} and Al^{3+}. Additionally, it is known that REE do not occupy octahedral sites in phyllosilicates (where Al, Fe and Mg are the main cations) but rather occupy adsorption sites of larger coordination and size (Laveuf and Cornu, 2009; Borst et al., 2020).

Other possible site in jarosite and alunite where REE could be lodged is the 12-fold coordinated K position. We assessed the radius of K^+ from published K—O distances (Kato and Miura, 1977; Sato et al., 2009) by subtracting the radius of the oxide anion in octahedral coordination (1.4 Å, as a trade-off between the smaller value of the coordinating hydroxyls in jarosite and alunite, and the larger value expected in 12-fold coordination; Shannon, 1976). This 12-fold coordination site is larger and can accommodate all REE according to their calculated ionic radii (Fig. 10b). Accordingly, LREE are likely to be preferentially retained in this site, as observed, because the size of the site is closest to their radii. The maximum concentration of Nd—Sm in alunite (Fig. 10a), also reported previously (Deyell et al., 2005; Martínez et al., 2006), could equally be explained by the crystallographic site occupied by the REE. The 12-fold coordination site is ~0.05 Å larger in jarosite than in alunite (Fig. 10b). Calculated radii of some LREE show ionic radii always smaller than the corresponding radius of K in both jarosite and alunite. However, calculated crystal radii of La and Ce are larger than that of K in alunite (Shannon, 1976). This suggests the possibility that the REE that best fit the 12-fold site in alunite, in substitution for K, are somewhere between Ce and Eu, which causes the higher concentration of these elements in alunite. In jarosite, the best fit is for La and all other REE are in lower concentration. It is impossible to analyze the fit completely because several adjustments are likely to take place to balance the excess positive charge created by the Ln^{3+} for K^+ substitution, such as loss of protons by some of the four hydroxyls coordinating the cation or,

perhaps, creation of some cation vacancies. These adjustments most probably modify the size of sites occupied by REE. It is the relative size of the calculated radii of REE to those of the 12-fold coordination site in jarosite and alunite which suggest the cause of the different REE relative concentrations in these two minerals.

This is a first-order interpretation of the REE patterns in alunite and jarosite because they could be complicated by factors such as successive dissolution-precipitation events, equilibrium/disequilibrium between the fluids and the dissolving rock or the precipitating new minerals (in equilibrium, the patterns of REE in rock and fluids tend to be complementary, but this is not the case far from equilibrium) or the existence/precipitation of trace phosphates in a few of our samples, which are resistant to dissolution and concentrate REE (Deyell et al., 2005). For example, data of REE content in leaching acidic fluids, rather than from the rocks, in experiments leaching andesitic rocks (Kikawada et al., 1995) and in concentrated acidic hydrothermal waters in Yellowstone (Lewis et al., 1997) both show moderate LREE enrichment over HREE. Such segregation may influence REE composition of secondary phases.

Goethite content in the samples does not correlate well with any REE variable (Fig. 7). The closest, but weak, link is to the REE slope. The literature does not provide as much information on goethite REE patterns as it does on jarosite and alunite. de Oliveira and Imbernon (1998) found no vertical modification of REE patterns in a lateritic profile from the weathered saprolite, dominated by goethite, plumbogummite-group minerals and quartz, to the fresh rock consisting of phoscorite with abundant carbonatitic veins. However, in this case the phosphates, rather than goethite, probably controlled the REE concentrations. Also in a lateritic profile, Ulrich et al. (2019) found that modifications of the REE patterns from the original ophiolite to the goethite-dominated horizon (~75 wt% goethite) consisted mainly in major changes to the individual concentration of Ce, probably due to redox conditions, and minor changes to the concentrations of Eu, Gd and Ho. Ulrich et al. (2019) interpreted that REE from the dissolving rock are approximately uniformly adsorbed on goethite and thus concentrated. Although not concluding, the above two references suggest that direct goethite formation from alteration of silicate rocks does not greatly modify the REE patterns other than concentrating them due to preferential retention on the altered rock over loss to altering fluids.

Fig. 6 indicated that samples dominated by sulfates and goethite tended to have a high REE slope and no Eu anomaly or a positive one, whereas Fig. 7 indicated that, overall (i.e., considering all goethite contents, high and low: see results), goethite concentration is independent of the Eu anomaly and only weakly correlated to the REE slope. This result is relevant to the two possible origins of goethite. Mavris et al. (2018) discussed that goethite in these samples may originate directly from acidic alteration at pH > 3 or from dissolution of jarosite (formed at pH < 3) after the pH of the fluids increased to circumneutral. Both processes are recognized in the gossan existing in some of the areas investigated here (Velasco et al., 2013). Thus, these two origins may cause two different REE patterns in goethite. If such was the case, the lack of correlation of goethite concentration with REE variables (Fig. 7) can be assigned to a mixed REE signal in goethite produced by the two different goethite origins. This possibility can be explored discussing those samples with high goethite concentration.

The two samples with highest goethite relative contents versus phyllosilicates and sulfates, are TH9 and TH5 (Table 1), with ~15 and ~37 wt% goethite (Cuadros et al., 2020). Compared with the original rock (TH12), the REE signature of TH9 shows no change (except for normalized REE abundance), whereas TH5 displays loss of the positive Eu anomaly and a continuous reduction of the HREE beyond Dy (Fig. 5). The fact that there was some kaolinite in TH5 suggests that it did not experience acidic alteration at pH < 3, where kaolinite would have dissolved completely. Rather, goethite probably formed as a first alteration product at pH > 3. The concentration of goethite in TH5 is much higher than that of kaolinite (Table 1), and it can be safely assumed that the REE signature of TH5 is that of goethite. On the contrary, sample TH9 contains no kaolinite and some jarosite, suggestive of acidic alteration at pH < 3. Here, goethite may be the product of late jarosite alteration after fluids became less acidic. As there is more goethite than jarosite in sample TH9 (Table 1), it is assumed that the REE patterns are controlled by goethite. Accordingly, the two possible paths of goethite formation in these two samples may have caused the two different goethite REE signatures observed. If such was the case, there is hope that REE could be used in the future to better constrain the set of processes originating goethite in geological settings. Alternatively, the lack of Eu anomaly in TH5 may be linked to its different location within Tharsis (Fig. 1) and be due to a local higher Eu concentration there.

5.4. REE pattern modifications differing from the general trends

Sample EV27 has an REE pattern which is very different from that of the original rock (EV2) and from most altered samples (Fig. 3). Sample EV27 is highly depleted in LREE although it preserves the negative Eu anomaly. Mineralogically, EV27 is different from all other samples in that it only contains major quartz and minor plagioclase/feldspar (Table 1). Thus, the REE patterns could represent the signature of quartz. This interpretation is supported by the REE patterns in sample EV10, which has a similar overall shape but with a less pronounced slope (Fig. 3). Sample EV10 contains major quartz and minor plagioclase/feldspar and kaolinite (Table 1), and thus, it is possible that the presence of kaolinite modifies the REE patterns. However, it is puzzling that sample EV10 does not display a Eu negative anomaly, which is present in every other sample from El Villar.

Samples from El Villar have another interesting feature. The two pairs of spatially consecutive samples EV5-EV6 and EV12-EV13 have Ce anomalies of opposite sign within each pair (Fig. 3). This strongly suggests that the same processes that concentrated Ce in EV6 and EV12 removed it from EV5 and EV13. Cerium anomalies are usually linked to redox processes (Liu et al., 2022). It can be hypothesized that oxidizing acidic fluids flowed from EV6 to EV5, and from EV12 to EV13. As these fluids dissolved the rock in EV6 and EV12 they also partially oxidized Ce^{3+} to Ce^{4+}, which precipitated in situ as CeO, while fluids transported the Ce-depleted REE suite into EV5 and EV13, where the REE were adsorbed on the kaolinite forming during the alteration process (Table 1). This explanation is coherent with two facts. First, that the concentration of REE is higher in EV5 than in EV6, and higher in EV13 than in EV12. Second, that where the Ce anomalies are deeper (EV5-EV6 pair) there is a greater difference of REE concentrations between the samples (Fig. 3). Both facts suggest that they are generated by the same process of fluids moving from EV6 to EV5 and from EV12 to EV13. The movement of fluids from EV6 to EV5 is also indicated by the mineralogy of the samples. Lower rock alteration is observed in EV5 (Table 1), consistent with fluids of reduced acidic activity after traversing EV6. Samples EV12 and EV13 have very similar mineralogy, but sample EV12 has more kaolinite than EV13 (Table 1), indicating also more acidic fluids in EV12 than in EV13.

In Quebrantahuesos, the alteration causes three different modifications, linked to location. One is REE concentration with no change in the pattern (beudantite-rich sample Q8; Figs. 1 and 4). Another is LREE >> HREE with loss of negative Eu anomaly (alunite-rich samples Q2, Q3, Q4). The third is loss of the negative Eu anomaly or development of a positive Eu anomaly (Q6, Q7, Q13; Figs. 1 and 4). The slope is not modified in the last case, even though there is alunite in Q6 and Q7 (Table 1), probably because illite (Q6 and Q7) and goethite (Q13), which are substantially abundant, are the main controls of the REE patterns. The problematic issue is how Eu relative concentration increased in these specimens. Samples Q6 and Q7 are from the same location (Fig. 1) and Q13 from a level above Q6 and Q7, closer to the pyrite causing the acidic alteration. The most direct explanation is that Eu-enriched fluids reached these samples. The fact that sample Q13, closer to the pyrite body, has higher relative Eu than Q6 and Q7 may point in this direction, although there is no known reason why the pyrite

body should generate percolating acidic fluids enriched in Eu alone.

In Tharsis, the rocks that underwent hydrothermal alteration (before the acidic alteration) were mainly shales, rather than volcanics as in all three other sites. This rock (TH12) displays a prominent positive Eu anomaly (Fig. 5). This Eu anomaly is maintained in all samples, including the jarosite-rich specimens TH10 and TH11 (characterized by their pattern with LREE > > HREE). The only sample that behaves differently from the main trends indicated by PCA (Figs. 7 and 8) is TH5, which lacks a Eu anomaly and does not have LREE > > HREE. Sample TH5 was collected from a different location within Tharsis from the rest (Fig. 1). This specimen has been considered above while discussing the effect of goethite in the general trends of modification of the REE patterns.

6. Conclusions

Acid-altered rocks from four locations from the Iberian Pyrite Belt (Calañas, El Villar, Quebrantahuesos, Tharsis) display a variety of REE patterns. In all cases, the original rocks (before acid alteration) had abundant phyllosilicates that were the main REE reservoir. These original rocks had formed by hydrothermal alteration of volcanics or shale precursors.

Where the precursor rocks were mainly volcanics (Calañas, El Villar, Quebrantahuesos) REE of the rock before acid alteration normalized to upper crust composition (McLennan, 2001) displayed patterns that ranged from flat to gently increasing towards HREE, always with a negative Eu anomaly. Where the precursor rocks were mainly shales (Tharsis), the REE patterns of the original rock were flat with a positive Eu anomaly.

The main characteristics of the REE patterns produced in the acid alteration and their interpretation are the following:

1) Alteration at pH 5–7. The alteration products are mainly phyllosilicates. The REE signature of the original rock is mostly preserved. This is interpreted as due to reduced fluid/rock ratio and mineral control of REE binding sites. Both inherited minerals and neoformed phyllosilicates have the same REE signature.
2) Alteration at pH 3–5. The main alteration products are kaolinite and alunite. Where alunite is most abundant, the REE patterns are completely modified to a pattern in which LREE are greatly enriched with respect to HREE (with a maximum at Nd—Sm and a steep downstep approximately between Sm and Tb). This modification is interpreted as due to a good fit of the size of the LREE 3+ cations to the 12-fold coordination site in alunite, and best for Nd and Sm.
3) Alteration at pH < 3. The alteration products were jarosite and beudantite. Only the case of jarosite was favorable for analysis. Jarosite samples displayed an approximately constant decrease of REE from Ce to Lu, except that the (positive) Eu anomaly from the precursor rock was preserved. This pattern is interpreted to be due to a best fit of the size of La^{3+} to the 12-fold coordination site in jarosite, with a progressively decreasing fit in the REE series to Lu.

Goethite appears as an alteration product with a variable REE signature. Such variability may be due to the two possible routes of goethite formation, one of which is precipitation during alteration of silicates at 7 > pH > 3, and the other consists of two steps, (1) formation of jarosite by alteration of silicates at pH < 3 and (2) precipitation of goethite by later alteration of jarosite at pH > 3.

The above interpretations of alunite, jarosite and goethite REE signatures are novel and provide models to understand such signatures as well as the basis to predict REE distributions from mineralogy in acidic environments and to use REE as tracers of geochemical processes more universally and efficiently.

Declaration of Competing Interest

The authors declare that they have no known competing financial interests or personal relationships that could have appeared to influence the work reported in this paper.

Data availability

Data are available in the Supplementary material (for REE) and in Deposit item AM-18-126330 at http://www.minsocam.org/MSA/AmMin/TOC/2018/Dec2018_data/Dec2018_data.html (for XRD).

Acknowledgments

Field trip and experimental work were funded by the European Commission (Marie Curie Fellowship “Acid-Mars” to C.M.). We thank Raquel Vega for assistance in the field and Gabriel R. P. Andrade for inspiration and discussions on REE retention in clays. We also thank two anonymous reviewers for insights and comments that helped to improve this article.

Appendix A. Supplementary data

Supplementary data to this article can be found online at https://doi.org/10.1016/j.chemgeo.2023.121323.

References

Adamides, N.G., 2013. Rio Tinto (Iberian Pyrite Belt): a world-class mineral field reopens. Appl. Earth Sci.: Trans. Inst. Min. Metall. B 122, 2–15.
Andrade, G.R.P., Cuadros, J., Barbosa, J.M.P., Vidal-Torrado, P., 2022. Clay minerals control rare earth elements (REE) fractionation in Brazilian mangrove soils. Catena 209, 105855. https://doi.org/10.1016/j.catena.2021.105855.
Ayora, C., Macías, F., Torres, E., Nieto, J.M., 2015. Rare earth elements in acid mine drainage. In: XXXV Reunión de la Sociedad Española de Mineralogía, Contribution S3, p. 22.
Borst, A.M., Smith, M.P., Finch, A.A., Estrade, G., Benavent, C.V., Nason, P., Marquis, E., Horsburgh, N.J., Goodenough, K.M., Xu, C., Kynicky, J., Geraki, K., 2020. Adsorption of rare earth elements in regolith-hosted clay deposits. Nat. Commun. 11, 4389. https://doi.org/10.1038/s41467-020-17801-5.
Brookins, D.G., 1989. Aqueous geochemistry of rare earth elements. In: Lipin, B.R., McKay, G.A. (Eds.), Geochemistry and Mineralogy of Rare Earth Elements. Reviews in Mineralogy, vol. 21. Mineralogical Society of America, Washington, pp. 201–225.
Capitán, A., Nieto, J.M., Sáez, R., Almodóvar, G.R., 2003. Caracterización textural y mineralógica del gossan de Filón Sur (Tharsis, Huelva). Bol. Soc. Esp. Mineral. 26, 45–58.
Chakhmouradian, A.R., Wall, F., 2012. Rare earth elements: Minerals, mines, magnets (and more). Elements 8, 333–340. https://doi.org/10.2113/gselements.8.5.333.
Cuadros, J., Manuel Sánchez-Marañón, M., Mavris, C., Fiore, S., Bishop, J.L., Melgosa, M., 2020. Color analysis and detection of Fe minerals in multi-mineral mixtures from acid-alteration environments. Appl. Clay Sci. 193, 105677 https://doi.org/10.1016/j.clay.2020.105677.
de Oliveira, S.M.B., Imbernon, R.A.L., 1998. Weathering alteration and related REE concentration in the Catalão I carbonatite complex, Central Brazil. J. S. Am. Earth Sci. 11, 379–388. https://doi.org/10.1016/S0895-9811(98)00024-8.
Deyell, C.L., Ryeb, R.O., Landisb, G.P., Bissig, T., 2005. Alunite and the role of magmatic fluids in the Tambo high-sulfidation deposit, El Indio–Pascua belt, Chile. Chem. Geol. 215, 185–218. https://doi.org/10.1016/j.chemgeo.2004.06.038.
Dutrizac, J.E., 2017. The behaviour of the rare earth elements during gypsum ($CaSO_4{\cdot}2H_2O$) precipitation. Hydrometallurgy 174, 38–46. https://doi.org/10.1016/j.hydromet.2017.09.013.
Essalhi, M., Sizaret, S., Barbanson, L., Chen, Y., Lagroix, F., Demory, F., Nieto, J.M., Saez, R., Capitán, M.A., 2011. A case study in the internal structure of the gossans and weathering processes in the Iberian Pyrite Belt using magnetic fabrics and paleomagnetic dating. Mineral. Deposita 46, 981–999.
Gimeno-Serrano, M.J., Auqué-Sanz, L.F., Nordstrom, D.K., 2000. REE speciation in low-temperature acidic waters and the competitive effects of aluminum. Chem. Geol. 165, 167–180.
He, Y., Zhang, Q., Shao, S., Zhu, X., Zhu, C., Wang, D., 2006. REE characteristics of the Fanshan alunite deposit in Zhejiang Province, China. Chin. J. Geochem. 25, 366–373.
Inguaggiato, C., Burbano, V., Rouwet, D., Garzon, G., 2017. Geochemical processes assessed by rare Earth elements fractionation at “Laguna Verde” acidic-sulphate crater lake (Azufral volcano, Colombia). Appl. Geochem. 79, 65–74. https://doi.org/10.1016/j.apgeochem.2017.02.013.
Inguaggiato, C., Pappaterra, S., Peiffer, L., Apollaro, C., Brusca, L., De Rosa, R., Rouwet, D., Caudrone, C., Suparjan, 2020. Mobility of REE from a hyperacid brine to

secondary minerals precipitated in a volcanic hydrothermal system: Kawah Ijen crater lake (Java, Indonesia). Sci. Total Environ. 740, 140133 https://doi.org/10.1016/j.scitotenv.2020.140133.
Kato, T., Miura, Y., 1977. The crystal structure of jarosite and svanbergite. Mineral. J. 8, 419–430.
Kikawada, Y., Oi, T., Ossaka, T., Kakihana, H., Honda, T., 1995. Leaching of lanthanoids from andesite rocks by acidic aqueous solutions. Geochem. J. 29, 67–84.
Kikawada, Y., Fukaia, M., Oia, T., 2013. Specific REE patterns observed in sulfurous hot springs from a hydrothermal alteration area in Manza, Japan. Proc. Earth Planet. Sci. 7, 428–431.
Kynicky, J., Smith, M.P., Xu, C., 2012. Diversity of rare earth deposits: the key example of China. Elements 8, 3361–3367. https://doi.org/10.2113/gselements.8.5.361.
Laveuf, C., Cornu, S., 2009. A review on the potentiality of rare earth elements to trace pedogenetic processes. Geoderma 154, 1–12. https://doi.org/10.1016/j.geoderma.2009.10.002.
Lewis, A.J., Palmer, M.R., Sturchio, N.C., Kemp, A.J., 1997. The rare earth element geochemistry of acid-sulfate and acid-sulfate-chloride geothermal systems from Yellowstone National Park, Wyoming, USA. Geochim. Cosmochim. Acta 61, 695–706.
Leybourne, M.I., Peter, J.M., Layton-Matthews, D., Volesky, J., Boyle, D.R., 2006. Mobility and fractionation of rare earth elements during supergene weathering and gossan formation and chemical modification of massive sulfide gossan. Geochim. Cosmochim. Acta 70, 1097–1112. https://doi.org/10.1016/j.gca.2005.11.003.
Liu, H., Guo, H., Pourret, O., Wang, Z., Sun, Z., Zhang, W., Liu, M., 2021. Distribution of rare earth elements in sediments of the North China Plain: a probe of sedimentation process. Appl. Geochem. 134, 105089 https://doi.org/10.1016/j.apgeochem.2021.105089.
Liu, X., Tournassat, C., Grangeon, S., Kalinichev, S., Takahashi, Y., Fernandes, M.M., 2022. Molecular-level understanding of metal ion retention in clay-rich materials. Nat. Rev. Earth Environ. 3, 461–476. https://doi.org/10.1038/s43017-022-00301-z.
Martínez, J.C., Dristas, J.A., Massonne, H.-J., Theye, T., 2006. Alunite and REE-rich APS minerals associated to the hydrothermal clay deposits in the Barker Area, Tandilia, Argentina. Clay Sci. 12 (2), 15–20.
Martin-Izard, A., Arias, D., Arias, M., Gumiel, P., Sanderson, D.J., Castañon, C., Lavandeira, A., Sanchez, J., 2015. A new 3D geological model and interpretation of structural evolution of the world-class Rio Tinto VMS deposit, Iberian Pyrite Belt (Spain). Ore Geol. Rev. 71, 457–476.
Mavris, C., Cuadros, J., Nieto, J.M., Bishop, J.L., Michalski, J.R., 2018. Diverse mineral assemblages of acidic alteration in the Rio Tinto area (Southwest Spain): Implications for Mars. Am. Mineral. 103, 1877–1890. https://doi.org/10.2138/am-2018-6330.
McLennan, S.M., 1989. Rare earth elements in sedimentary rocks: Influence of provenance and sedimentary processes. In: Lipin, B.R., McKay, G.A. (Eds.), Geochemistry and Mineralogy of Rare Earth Elements. Reviews in Mineralogy, vol. 21. Mineralogical Society of America, Washington, pp. 169–200.
McLennan, S.M., 2001. Relationships between the trace element composition of sedimentary rocks and upper continental crust. Geochem. Geophys. Geosyst. https://doi.org/10.1029/2000GC000109, 2000GC000109.
Mitjavila, J., Martí, J., Soriano, C., 1997. Magmatic evolution and tectonic setting of the Iberian Pyrite Belt volcanism. J. Petrol. 38, 727–755.
Mitra, S., Gupta, S., Mitra, K., Bhattacharya, S., Chakrabarti, R., Ray, D., Banerjee, S., Chauhan, P., Parthasarathy, G., 2017. Spectroscopic Signature and Geochemical Constraints on Jarosite Formation at Kachchh: Implications for Mars. Lunar and Planetary Science XLVIII. Abstract 2270.
Moore, D.M., Reynolds Jr., R.C., 1997. X-Ray diffraction and the identification and analysis of clay minerals, second ed. Oxford University Press, Oxford.
Ondrejka, M., Bačík, P., Sobocký, T., Uher, P., Škoda, R., Mikuš, T., Luptáková, L., Konečný, P., 2018. Minerals of the rhabdophane group and the alunite supergroup in microgranite: products of low-temperature alteration in a highly acidic environment from the Velence Hills, Hungary. Mineral. Mag. 82, 1277–1300. https://doi.org/10.1180/mgm.2018.137.
Parsapoor, A., Khalili, M., Mackizadeh, M.A., 2009. The behaviour of trace and rare earth elements (REE) during hydrothermal alteration in the Rangan area (Central Iran). J. Asian Earth Sci. 34, 123–134.
Pérez-López, R., Delgado, J., Nieto, J.M., Márquez-García, B., 2010. Rare earth element geochemistry of sulfide weathering in the São Domingos mine area (Iberian Pyrite Belt): a proxy for fluid–rock interaction and ancient mining pollution. Chem. Geol. 276, 29–40. https://doi.org/10.1016/j.chemgeo.2010.05.018.
Prudêncio, M.I., Figueiredo, M.O., Cabral, J.M.P., 1989. Rare earth distribution and its correlation with clay mineralogy in the clay-sized fraction of cretaceous and Pliocene sediments (Central Portugal). Clay Miner. 24, 67–74.
Roaldset, E., 1973. Rare earth elements in Quaternary clays of the Numedal area, southern Norway. Lithos 6, 349–372.
Romero, F.M., Prol-Ledesma, R.M., Canet, C., Núñez Alvares, L., Pérez-Vázquez, R., 2010. Acid drainage at the inactive Santa Lucia mine, western Cuba: Natural attenuation of arsenic, barium and lead, and geochemical behavior of rare earth elements. Appl. Geochem. 25, 716–727. https://doi.org/10.1016/j.apgeochem.2010.02.004.
Sato, E., Nakai, I.,, Miyawaki, R., Matsubara, S., 2009. Crystal Structures of alunite family minerals: beaverite, corkite, alunite, natroalunite, Jarosite, svanbergite, and woodhouseite. Neues Jahrb. für Mineral. Abhandlungen 185, 313–322. https://doi.org/10.1127/0077-7757/2009/0128.
Schijf, J., Byrne, R.H., 2004. Determination of $_{SO4}\beta_1$ for yttrium and the rare earth elements at I=0.66 m and t=25°C—Implications for YREE solution speciation in sulfate-rich waters. Geochim. Cosmochim. Acta 68, 2825–2837.
Shannon, R.D., 1976. Revised effective ionic radii and systematic studies of interatomic distances in halides and chalcogenides. Acta Crystallogr. A32, 751–767.
Terekado, Y., Fujitani, T., 1998. Behavior of the rare earth elements and other trace elements during interactions between acidic hydrothermal solutions and silicic volcanic rocks, southwestern Japan. Geochim. Cosmochim. Acta 62, 1903–1917.
Tornos, F., 2006. Environment of formation and styles of volcanogenic massive sulfides: the Iberian Pyrite Belt. Ore Geol. Rev. 28, 259–307.
Tornos, F., Solomon, M., Conde, C., Spiro, B.F., 2008. Formation of the Tharsis massive sulfide deposit, Iberian Pyrite Belt: geological, lithogeochemical, and stable isotope evidence for deposition in a brine pool. Econ. Geol. 103, 185–214.
Toscano, M., Pascual, E., Nesbitt, R.W., Donaire, T., 2014. Geochemical discrimination of hydrothermal and igneous zircon in the Iberian Pyrite Belt, Spain. Ore Geol. Rev. 56, 301–311.
Ulrich, M., Cathelineau, M., Muñoz, M., Boiron, M.-C., Teitler, Y., Karpoff, A.M., 2019. The relative distribution of critical (Sc, REE) and transition metals (Ni, Co, Cr, Mn, V) in some Ni-laterite deposits of New Caledonia. J. Geochem. Explor. 197, 93–113. https://doi.org/10.1016/j.gexplo.2018.11.017.
Velasco, F., Herrero, J.M., Suárez, S., Yusta, I., Alvaro, A., Tornos, F., 2013. Supergene features and evolution of gossans capping massive sulfide deposits in the Iberian Pyrite Belt. Ore Geol. Rev. 53, 181–203. https://doi.org/10.1016/j.oregeorev.2013.01.008.
Welch, S.A., Christy, A.G., Isaacson, L., Kirste, D., 2009. Mineralogical control of rare earth elements in acid sulfate soils. Geochim. Cosmochim. Acta 73, 44–64. https://doi.org/10.1016/j.gca.2008.10.017.